

---

# GEAR: Geometry-Aware Rényi Information

---

Jose Gallego,\* Ankit Vani, Max Schwarzer, Simon Lacoste-Julien<sup>†</sup>  
 Mila and DIRO, Université de Montréal

## Abstract

Shannon’s seminal theory of information has been of paramount importance in the development of modern machine learning techniques. However, standard information measures deal with probability distributions over an alphabet considered as a mere set of symbols and disregard further geometric structure, which might be available in the form of a metric or similarity function. We advocate the use of a notion of entropy that reflects not only the relative abundances of symbols but also the similarities between them, which was originally introduced in theoretical ecology to study the diversity of biological communities. Echoing this idea, we propose a criterion for comparing two probability distributions (possibly degenerate and with non-overlapping supports) that takes into account the geometry of the space in which the distributions are defined. Our proposal exhibits performance on par with state-of-the-art methods based on entropy-regularized optimal transport, but enjoys a closed-form expression and thus a lower computational cost. We demonstrate the versatility of our proposal via experiments on a broad range of domains: computing image barycenters, approximating densities with a collection of (*super*-) samples; summarizing texts; assessing mode coverage; as well as training generative models.

## 1 Introduction

We present GEometry-Aware Rényi (GEAR) information measures, a perspective on information theory which naturally incorporates the structure of the space in which the observations are embedded, be this a metric or a similarity space. These geometry-aware information measures were originally proposed by [1] for use in theoretical ecology where inter-species similarities play a crucial role in assessing of the diversity of an ecosystem, and are generalizations of the Rényi entropy [2]. This stands in contrast to Shannon’s theory of information [3], which is independent of the alphabet at hand, and depends only on the relative abundance of each symbol. Thus, information theory concepts derived from the Shannon entropy (such as cross entropy and the Kullback-Leibler divergence) are blind to the geometric structure in the domains over which the distributions are defined.

In this paper, we advocate the use of these geometry-aware measures in machine learning. We present the geometrically-aware entropy of [1] along with several important properties that connect it to fundamental notions in geometry. We also propose a training objective inspired by this notion of entropy, which compares two probability distributions by taking into account the similarities among the objects on which they are defined. Our proposal shares the empirical performance properties of distances based on optimal transport theory, such as the Wasserstein distance [4], but has the advantage of enjoying a closed-form expression. This helps reduce computation significantly, by obviating the need to solve a linear program or use matrix scaling algorithms [5]. We hope that these methods can prove fruitful in extending frameworks such as the information bottleneck for representation learning [6], similarity-sensitive cross entropy objectives for training classifiers in the spirit of loss-calibrated decision theory, or the use of entropic regularization of policies in reinforcement learning [7].

\*Contact: gallegoj@mila.quebec

<sup>†</sup>Canada CIFAR AI Chair

**Contributions.** The main contributions of this work are twofold. First, we introduce a geometry-aware notion of entropy to machine learning. Second, we propose a discrepancy inspired by this entropy, which allows the incorporation of geometric information when comparing probability distributions much as in optimal transport, but which has a closed-form expression.

**Paper structure.** We introduce the theory behind GEAR information measures, and provide motivating examples justifying their use. We then introduce and characterize a divergence-like loss derived from GEAR information. Finally, we demonstrate applications of our methods, including training generative models, approximating measures, finding barycenters, and supersampling distributions. We also show that our entropy definition can be used to evaluate the diversity of samples produced by generative models.

**Notation.** Calligraphic letters denote Sets, bold letters represent Matrices and vectors, and double-barred letters denote Probability distributions and information-theoretic functionals. To emphasize certain computational aspects, we alternatively denote a distribution  $\mathbb{P}$  over a finite space  $\mathcal{X}$  as a vector of probabilities  $\mathbf{p}$ .  $\mathbf{I}$ ,  $\mathbf{1}$  and  $\mathbf{J}$  denote the identity matrix, a vector of ones and matrix of ones, with context-dependent dimensions. For vectors  $\mathbf{v}$ ,  $\mathbf{u}$  and  $\alpha \in \mathbb{R}$ ,  $\frac{\mathbf{v}}{\mathbf{u}}$  and  $\mathbf{v}^\alpha$  denote element-wise division and exponentiation.  $\langle \cdot, \cdot \rangle$  denotes the Frobenius inner-product between two vectors or matrices.  $\delta_x$  denotes a Dirac distribution at point  $x \in \mathcal{X}$ .  $\Delta_n \triangleq \{\mathbf{x} \in \mathbb{R}^{n+1} \mid \langle \mathbf{1}, \mathbf{x} \rangle = 1 \text{ and } x_i \geq 0\}$  denotes the probability simplex over  $n$  elements. For a continuous map  $f : \mathcal{X} \rightarrow \mathcal{Y}$  and a measure  $\mathbb{P}$  on  $\mathcal{X}$ ,  $f\#\mathbb{P}$ , denotes the push-forward measure of  $\mathbb{P}$  induced by  $f$  over  $\mathcal{Y}$ , with samples obtained by applying  $f$  on  $x \sim \mathbb{P}$ . We adopt the conventions  $0 \cdot \log(0) = 0$  and  $x \log(0) = -\infty$  for  $x > 0$ .

**Reproducibility.** The code required to reproduce our experiments can be found here: <https://www.dropbox.com/sh/19vhg0nuqg823e/AADxhGwB0h7vjuqovwOLSPxZa>

## 2 Geometry-Aware Information Measures

Suppose that we are given a finite space  $\mathcal{X}$  with  $n$  elements along with a symmetric function that measures the similarity between elements,  $\kappa : \mathcal{X} \times \mathcal{X} \rightarrow [0, 1]$ . Let  $\mathbf{K}$  be the Gram matrix induced by  $\kappa$  on  $\mathcal{X}$ ; i.e.,  $\mathbf{K}_{x,y} \triangleq \kappa_{xy} \triangleq \kappa(x, y) = \kappa(y, x)$ .  $\mathbf{K}_{x,y} = 1$  indicates that the elements  $x$  and  $y$  are identical, while  $\mathbf{K}_{x,y} = 0$  indicates full dissimilarity. We call  $(\mathcal{X}, \kappa)$  a (finite) similarity space. For brevity we denote  $(\mathcal{X}, \kappa)$  by  $\mathcal{X}$  whenever  $\kappa$  is clear from the context.

Of particular importance are the similarity spaces arising from metric spaces. Let  $(\mathcal{X}, d)$  be a metric space and define  $\kappa(x, y) \triangleq e^{-d(x, y)}$ . Here, the symmetry and range conditions imposed on  $\kappa$  are trivially satisfied. The triangle inequality in  $(\mathcal{X}, d)$  induces a multiplicative transitivity on  $(\mathcal{X}, \kappa)$ : for all  $x, y, z \in \mathcal{X}$ ,  $\kappa(x, y) \geq \kappa(x, z)\kappa(z, y)$ . Moreover, for any (non-degenerate) metric space, the Gram matrix of its associated similarity space is positive definite [8, Lemma 2.5].

Note that there is an implicit choice of scale in the basis of the exponent in the definition of the similarity function. In fact, for each metric space we have a family of similarity spaces indexed by a scale parameter  $\sigma$ : define  $\kappa_\sigma(x, y) \triangleq e^{-\frac{d(x, y)}{\sigma}}$ . This is a central concept in the theory of the magnitude (a refined notion of size) of a metric space developed in [9].

In this section, we develop a theoretical framework which allows us to quantify the “diversity” or “entropy” of a probability distribution defined on a similarity space, as well as a criterion for comparing distributions on such spaces. Because of the connection between metric spaces (the canonical notion of geometry) and similarity spaces (our operational tool), we qualify the information-theoretic concepts presented below as *geometry-aware*.

### 2.1 Entropy and diversity

Let  $\mathbb{P}$  be a probability distribution on  $\mathcal{X}$ .  $\mathbb{P}$  induces a *similarity profile*  $\mathbf{K}\mathbb{P} : \mathcal{X} \rightarrow [0, 1]$ , given by  $\mathbf{K}\mathbb{P}(x) \triangleq \mathbb{E}_{y \sim \mathbb{P}} [\kappa(x, y)] = (\mathbf{K}\mathbf{p})_x$ .<sup>3</sup>  $\mathbf{K}\mathbb{P}(x)$  represents the expected similarity between element  $x$  and a random element of the space sampled according to  $\mathbb{P}$ . Intuitively, it assesses how “satisfied” we would be by selecting  $x$  as a one-point summary of the space. In other words, it measures the ordinarity of  $x$ , and thus  $\frac{1}{\mathbf{K}\mathbb{P}(x)}$  is the rarity or *distinctiveness* of  $x$  [1]. Note that the distinctiveness depends crucially on both the similarity structure of the space and the probability distribution at hand.

<sup>3</sup>This is the  $x$ -th entry of the result of the matrix-vector multiplication  $\mathbf{K}\mathbf{p}$ .

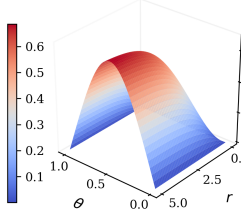


Figure 1:  $\mathbb{H}_1^K$  interpolates towards Shannon's entropy.

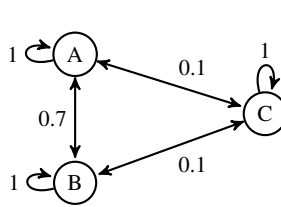


Figure 2: A 3-point space with two highly similar elements.

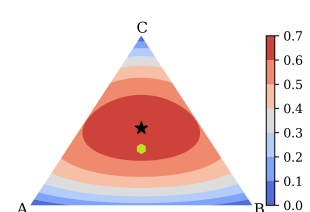


Figure 3: Entropy heatmap of the space in Figure 2.

Much like the interpretation of Shannon's entropy as the expected surprise of observing a random element of the space, we can define a notion of diversity as *expected distinctiveness*:  $\sum_{x \in \mathcal{X}} \mathbb{P}(x) \frac{1}{\mathbf{K}\mathbb{P}(x)}$ . This arithmetic weighted average is a particular instance of the family of aggregation functions called power (or Hölder) means: given  $\mathbf{w} \in \Delta_n$  and  $\mathbf{x} \in \mathbb{R}_{\geq 0}^n$ , the *weighted power mean of order  $\beta$*  is defined as  $M_{\mathbf{w}, \beta}(\mathbf{x}) \triangleq \langle \mathbf{w}, \mathbf{x}^\beta \rangle^{\frac{1}{\beta}}$ . This averaging scheme motivated the following definition by [1]:

**Definition 1.** [1] **(GEAR Entropy)** *The geometry-aware Rényi entropy of order  $\alpha \geq 0$  of a distribution  $\mathbb{P}$  on a finite similarity space  $(\mathcal{X}, \kappa)$  is given by:*

$$\mathbb{H}_\alpha^K[\mathbb{P}] \triangleq \log M_{\mathbf{p}, 1-\alpha} \left( \frac{1}{\mathbf{K}\mathbf{p}} \right) = \frac{1}{1-\alpha} \log \sum_{i=1}^n \mathbf{p}_i \frac{1}{(\mathbf{K}\mathbf{p})_i^{1-\alpha}} = \frac{1}{1-\alpha} \log \langle \mathbf{p}, (\mathbf{K}\mathbf{p})^{\alpha-1} \rangle. \quad (1)$$

It is evident that whenever  $\mathbf{K} = \mathbf{I}$ , this definition reduces to the Rényi entropy [2]. Moreover, a continuous extension of Eq. (1) to  $\alpha = 1$  reveals a similarity-sensitive version of Shannon's entropy.<sup>4</sup>

Let us dissect this definition via two simple examples. First, consider a distribution  $\mathbf{p}_\theta = [\theta, 1-\theta]^T$  on a metric space consisting of two points  $\{x, y\}$  at a distance  $r$  from each other, and define the similarity  $\kappa_{xy} \triangleq e^{-r}$ . As the points get further apart, the Gram matrix  $\mathbf{K}_r$  transitions from  $\mathbf{J}$  to  $\mathbf{I}$ . Fig. 1 displays the behavior of  $\mathbb{H}_1^K[\mathbf{p}_\theta]$ . We observe that when  $r$  is large, we recover the familiar shape of Shannon's entropy for a Bernoulli distribution. On the other hand, for low values of  $r$  the curve is close to a constant zero function. In this case, we regard both elements of the space as almost identical; thus, no matter how we distribute the probability mass among them, we have low uncertainty on the qualities of random observations. Moreover, the exponential of the maximum entropy,  $\sup_\theta \exp \mathbb{H}_1^K[\mathbf{p}_\theta] = 1 + \tanh(r) \in [1, 2]$ , measures the *effective number of points* in  $\mathcal{X}$  at scale  $r$  [10].

Now, consider the space presented in Fig. 2, with edge weights denoting the similarity between elements. The maximum entropy distribution in this space following Shannon's theory is the uniform distribution  $\mathbf{u} = [\frac{1}{3}, \frac{1}{3}, \frac{1}{3}]^T$ . This is counter-intuitive when we take into account the fact that points A and B are very similar. We argue that a reasonable expectation for a maximum entropy distribution is one which allocates roughly probability  $\frac{1}{2}$  to point C and the remaining mass in equal proportions to points A and B. Fig. 3 displays the value of  $\mathbb{H}_1^K$  for all distributions on the 3-simplex. The green dot represents  $\mathbf{u}$ , while the black star corresponds to the maximum GEAR entropy with [A, B, C]-coordinates  $\mathbf{p}^* \triangleq [0.273, 0.273, 0.454]^T$ . The induced similarity profile is  $\mathbf{K}\mathbf{p}^* = [\frac{1}{2}, \frac{1}{2}, \frac{1}{2}]^T$ . Note how Shannon's mass-uniformity gets translated into uniformity on the similarity profile.

**Properties.** We now list several important properties satisfied by the GEAR entropy, whose proofs and formal statements are contained in [1] and [10]:

- **Range:** For any distribution  $\mathbb{P} \in \Delta_n$ , we have  $0 \leq \mathbb{H}_\alpha^K[\mathbb{P}] \leq \log(n)$
- **K-monotonic:** Increasing the similarity between the elements reduces the entropy. Formally, if  $\kappa_{xy} \geq \kappa'_{xy}$  for all  $x, y \in \mathcal{X}$ , then for all  $\mathbb{P} \in \Delta_{|\mathcal{X}|}$ ,  $\mathbb{H}_\alpha^K[\mathbb{P}] \leq \mathbb{H}_{\alpha'}^{\mathbf{K}'}[\mathbb{P}] \leq \mathbb{H}_\alpha^{\mathbf{I}}[\mathbb{P}]$ .
- **Modularity:** If the space is partitioned into fully dissimilar groups,  $(\mathcal{X}, \kappa) = \bigotimes_{c=1}^C (\mathcal{X}_c, \kappa_c)$ , so that the resulting  $\mathbf{K}$  is a block matrix ( $x \in \mathcal{X}_c, y \in \mathcal{X}_{c'}, c \neq c' \Rightarrow \kappa_{xy} = 0$ ), then the entropy of a distribution on  $\mathcal{X}$  is a weighted average of the block-wise entropies.
- **Symmetry:** Entropy is invariant under relabeling of the elements, provided that the rows of  $\mathbf{K}$  are permuted accordingly.

<sup>4</sup>A standard L'Hôpital argument yields  $\mathbb{H}_1^K[\mathbb{P}] = -\langle \mathbf{p}, \log(\mathbf{K}\mathbf{p}) \rangle$ .

- **Absence:** The entropy of a distribution  $\mathbb{P}$  over  $(\mathcal{X}, \kappa)$  remains unchanged when we restrict the similarity space to the support of  $\mathbb{P}$ .
- **Identical elements:** If two elements are identical (two equal rows in  $\mathbf{K}$ ), then combining them into one and adding their probabilities leaves the entropy unchanged.
- **Continuity:**  $\mathbb{H}_\alpha^\mathbf{K}[\mathbb{P}]$  is continuous in  $\alpha \in [0, \infty]$  for fixed  $\mathbb{P}$ , and continuous in  $\mathbb{P}$  (w.r.t. standard topology on  $\Delta$ ) for fixed  $\alpha \in (0, \infty)$ .
- **$\alpha$ -Monotonicity:**  $\mathbb{H}_\alpha^\mathbf{K}[\cdot]$  is a non-increasing function of  $\alpha$ .

**The role of  $\alpha$ .** Definition 1 establishes a family of entropies indexed by a non-negative parameter  $\alpha$ , which determines the relative importance of rare elements versus common ones (where rarity is quantified by  $\frac{1}{\mathbf{K}\mathbb{P}}$ ). In particular,  $\mathbb{H}_0^\mathbf{K}[\mathbb{P}] = \log \left\langle p, \frac{1}{\mathbf{K}\mathbb{P}} \right\rangle$ . When  $\mathbf{K} = \mathbf{I}$ ,  $\mathbb{H}_0^\mathbf{K}[\mathbb{P}] = \log |\text{supp}(\mathbb{P})|$ , which values rare and common species equally, while  $\mathbb{H}_\infty^\mathbf{K}[\mathbb{P}] = -\log \max_{i \in \text{supp}(\mathbb{P})} (\mathbf{K}\mathbb{P})_i$  only considers the most common element(s). Thus, in principle, the problem of finding a maximum entropy distribution depends on the choice of  $\alpha$ .

**Theorem 1.** [10] Let  $(\mathcal{X}, \kappa)$  be a similarity space. There exists a probability distribution  $\mathbb{P}_\mathcal{X}^*$  that maximizes  $\mathbb{H}_\alpha^\mathbf{K}[\cdot]$  for all  $\alpha \in \mathbb{R}_{\geq 0}$ , simultaneously. Moreover,  $\mathbb{H}_\mathcal{X}^* \triangleq \sup_{\mathbb{P} \in \Delta_{|\mathcal{X}|}} \mathbb{H}_\alpha^\mathbf{K}[\mathbb{P}]$  is independent of  $\alpha$ .

Remarkably, Theorem 1 shows that the maximum entropy distribution is independent of  $\alpha$ . Thus, the maximum value of the GEAR entropy is an intrinsic property of the space. In other words, this quantity is a *geometric invariant*. Indeed, if  $\kappa(x, y) \triangleq e^{-d(x, y)}$  for a metric  $d$  on  $\mathcal{X}$ , there exist deep connections between  $\mathbb{H}_\mathcal{X}^*$  and the magnitude of the metric space  $(\mathcal{X}, d)$  [9].

**Theorem 2.** [10] Let  $\mathbb{P}$  be a distribution on a similarity space  $(\mathcal{X}, \kappa)$ .  $\mathbb{H}_\alpha^\mathbf{K}[\mathbb{P}]$  is independent of  $\alpha$  if and only if  $\mathbf{K}\mathbb{P}(x) = \mathbf{K}\mathbb{P}(y)$  for all  $x, y \in \text{supp}(\mathbb{P})$ .

Recall the behavior of the similarity profile observed for  $\mathbf{p}^*$  in Fig. 2. Theorem 2 shows that this is not a coincidence: inducing a similarity profile with equal values in all of the entries that are part of the support of a distribution  $\mathbb{P}$  is a necessary condition for being a maximum entropy distribution. In the setting  $\alpha = 1$  and  $\mathbf{K} = \mathbf{I}$ , the condition  $\mathbf{K}\mathbb{P} = \mathbf{p} = \lambda\mathbf{1}$  for some  $\lambda \in \mathbb{R}_{\geq 0}$ , is equivalent to the well known fact that the uniform distribution maximizes Shannon entropy.

To the best of our knowledge, there is no characterization of the concavity of the landscape in the maximum entropy optimization problem discussed above. [10] present an algorithm with an exponential run-time to find *exact* maximizers. We exploit the fact that the objective is amenable to gradient-based optimization techniques and conduct experiments in spaces with thousands of elements. We observe reliable optimization results indicated by low variance in the objective value at convergence across random initializations (and random values of  $\alpha$  by virtue of Theorem 1), thus providing an efficient alternative for finding approximate maximum-entropy distributions. Details are presented in Appendix B.

## 2.2 Comparing probability distributions

Inspired by the framework discussed in the previous section, we propose the following criterion for comparing two probability distributions:

**Definition 2. (GEAR Discrepancy)** The geometry-aware Rényi discrepancy of order  $\alpha \geq 0$  between distributions  $\mathbb{P}$  and  $\mathbb{Q}$  on a finite similarity space  $(\mathcal{X}, \kappa)$  is given by:

$$\mathbb{D}_\alpha^\mathbf{K}[\mathbb{P}, \mathbb{Q}] = \frac{1}{2} \frac{1}{\alpha - 1} \left[ \log \left( \mathbf{p}^T \left( \frac{\mathbf{K}\mathbb{P}}{\mathbf{K}\mathbb{Q}} \right)^{\alpha-1} \right) + \log \left( \mathbf{q}^T \left( \frac{\mathbf{K}\mathbb{Q}}{\mathbf{K}\mathbb{P}} \right)^{\alpha-1} \right) \right] \quad (2)$$

In a similar fashion as the entropy, the criterion defined in Eq. (2) is a similarity-sensitive extension of the symmetrized Rényi divergence between  $\mathbb{P}$  and  $\mathbb{Q}$ , realized in the case  $\mathbf{K} = \mathbf{I}$ . If, in addition to this,  $\alpha = 1$ , we recover the symmetrized Kullback-Leibler divergence. Compared to the family of  $f$ -divergences [11], this definition computes point-wise ratios between the similarity profiles  $\mathbf{K}\mathbb{P}$  and  $\mathbf{K}\mathbb{Q}$  rather than the probability masses (or more generally, Radon-Nikodym w.r.t. a reference measure). Note how  $\mathbf{K}\mathbb{P}(x)$  involves a *global* view of the space via the Gram matrix from the perspective of  $x \in \mathcal{X}$ . We note that the symmetrized definition of the discrepancy is necessary, as the

unidirectional version can attain negative values in cases where  $q$  exploits  $\mathbf{K}$  more efficiently than  $p$ . Appendix C provides empirical evidence in the case of a standard RBF and a polynomial kernel supporting the conjecture that the symmetrized discrepancy is non-negative.

**Empirical distributions.** Although we have developed our discrepancy in the setting of distributions over a finite similarity space, we can effectively compare two empirical distributions over a continuous space. Note that if an arbitrary  $x \in \mathcal{X}$  (or more generally a measurable set  $E$  for a given choice of  $\sigma$ -algebra) has measure zero under both  $\mu$  and  $\nu$ , then such  $x$  ( $E$ ) is irrelevant in the computation of  $\mathbb{D}_\alpha^{\mathbf{K}}[\mathbb{P}, \mathbb{Q}]$ . Thus, when comparing empirical measures, the possibly continuous expectations involved in the extension of Eq. (2) to general measures reduce to finite sums over the corresponding supports.

Concretely, let  $(\mathcal{X}, \kappa)$  be a (possibly continuous) similarity space and consider the empirical distributions  $\mathbb{P} = \sum_{j=1}^m \mathbf{p}_j \delta_{y_j}$  and  $\mathbb{Q} = \sum_{i=1}^n \mathbf{q}_i \delta_{x_i}$  with  $\mathbf{p} \in \Delta_m$  and  $\mathbf{q} \in \Delta_n$ . The Gram matrix of the restriction of  $(\mathcal{X}, \kappa)$  to  $\mathcal{S} \triangleq \text{supp}(\mathbb{P}) \cup \text{supp}(\mathbb{Q})$  has the block structure  $\mathbf{K}_{\mathcal{S}} \triangleq \begin{pmatrix} \mathbf{K}_{xx} & \mathbf{K}_{xy} \\ \mathbf{K}_{yx} & \mathbf{K}_{yy} \end{pmatrix}$ , where  $\mathbf{K}_{xx}$  is  $m \times m$ ,  $\mathbf{K}_{yy}$  is  $n \times n$  and  $\mathbf{K}_{xy} = \mathbf{K}_{yx}^T$ . Straightforward linear algebra yields:

$$\mathbb{D}_\alpha^{\mathbf{K}}[\mathbb{P}, \mathbb{Q}] = \frac{1}{2\alpha-1} \left[ \log \left( \mathbf{p}^T \left( \frac{\mathbf{K}_{xx}\mathbf{p}}{\mathbf{K}_{xy}\mathbf{q}} \right)^{\alpha-1} \right) + \log \left( \mathbf{q}^T \left( \frac{\mathbf{K}_{yy}\mathbf{q}}{\mathbf{K}_{yx}\mathbf{p}} \right)^{\alpha-1} \right) \right] \quad (3)$$

**Complexity.** The computation of Eq. (3) requires  $\mathcal{O}(|\kappa|(m+n)^2)$  operations, where  $|\kappa|$  represents the cost of a kernel evaluation. While this exhibits a quadratic behavior in the size of the union of the supports, the result of this expression is already a quantitative assessment of the dissimilarity between  $\mathbb{P}$  and  $\mathbb{Q}$ . Note that the computation of our expression does not resort to the execution of several iterations of matrix scaling algorithms. The proposals of [12, 13] require at least  $\Omega((|\kappa| + L)mn)$  computations, where  $L$  denotes the number of Sinkhorn iterations, which is an increasing function of the desired optimization tolerance.

**Weak topology.** A desirable property of such a discrepancy for training neural generative models is the induction of a weak topology on the space of measures that results in useful gradients for learning. In Appendix A, we show that the GEAR discrepancy can provide a smooth training signal despite the disjointness in the supports of the model and target distributions.

### 3 Related work

**Theories of Information.** Information theory is ubiquitous in modern machine learning: from variable selection via information gain in decision trees [14], to using entropy as a regularizer in reinforcement learning [7], to rate-distortion theory for training generative models [15]. To the best of our knowledge, the work of Leinster [1, 10] is the first formal treatment of information-theoretic concepts in spaces with non-trivial geometry, albeit in the context of ecology.

**Comparing distributions.** The ability to compare probability distributions is at the core of statistics and machine learning. Although traditionally dominated by maximum likelihood estimation, a significant portion of the research on parameter estimation has shifted towards methods based on optimal transport, such as the Wasserstein distance [4]. Two main reasons for this transition are (i) the need to deal with degenerate distributions (which might have density only over a low dimensional manifold) as is the case in the training of generative models [16–18]; and (ii) the development of alternative formulations and relaxations of the original optimal transport objective which make it feasible to approximately compute in practice [12, 19].

**Relation to kernel theory.** The theory we have presented in this paper revolves around a notion of similarity on  $\mathcal{X}$ . The operator  $\mathbf{K}\mathbb{P}$  corresponds to the embedding of the space of distributions on  $\mathcal{X}$  into a reproducing kernel Hilbert space used for comparing distributions without the need for density estimation [20]. In particular, a key concept in this work is that of a characteristic kernel, i.e., a kernel for which the embedding is injective. Note that this condition is equivalent to the positive definiteness of the Gram matrix  $\mathbf{K}$  imposed above. Under these circumstances, the metric structure present in the Hilbert space can be imported to define the Maximum Mean Discrepancy distance between distributions [21]. Our definition of discrepancy also makes use of the object  $\mathbf{K}\mathbb{P}$  but has motivations rooted in information theory rather than functional analysis. We believe that the framework proposed in this paper has the potential to foster connections between both fields.

## 4 Experiments

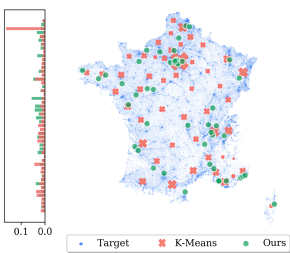


Figure 4: Approximating a discrete measure with a uniform empirical measure.

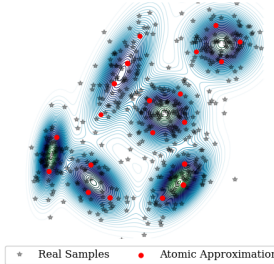


Figure 5: Approximating continuous measure with a finite set of approximate samples.

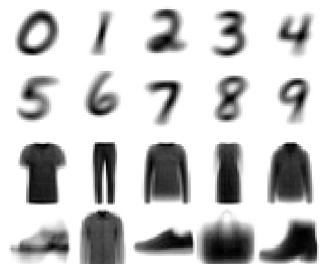


Figure 6: Barycenters for each class of MNIST and Fashion-MNIST.

### 4.1 Approximating measures and computing image barycenters

Our method allows us to approximate both discrete and continuous measures with finite samples by minimizing  $\mathbb{D}_\alpha^K$  with respect to the locations of the approximating atoms. In Fig. 4, we show the results of such an approximation on data for the population of France in 2010 consisting of 36,318 datapoints [22], similar to the setting of [12]. The weight of each location in the blue measure is proportional to the population it represents. Our approximating measure consists of 50 points with uniform weights. We compare with K-means [23] using identical initialization. Note that when using K-means, the resulting allocation of mass from points in the target measure to the nearest “centroid” can result in a highly unbalanced distribution, shown in the lateral bar plot. In contrast, our objective allows a uniformity constraint on the centroids, inducing a more homogeneous allocation.

Fig. 5 shows the approximation of a mixture of Gaussians by a uniform distribution over 20 atoms similar to the approximate super-samples [24] obtained by [25] using the Wasserstein distance. In the case of a continuous measure, we estimate the expectation by repeatedly sampling discrete minibatches to construct an empirical measure, and use gradient-based optimization to minimize  $\mathbb{D}_\alpha^K$  with respect to the location of the atoms of the approximating measure. Note how the result avoids oversampling dense regions observed in real samples and better approximates the density.

Fig. 6 shows the result of gradient-based optimization to find barycenters for each of the classes in MNIST [26] and Fashion-MNIST [27]. Given a collection of measures  $\mathcal{P} = \{\mathbb{P}_i\}_{i=1}^n$  on a similarity space, we define the barycenter of  $\mathcal{P}$  with respect to the GEAR discrepancy as the minimizer of  $\frac{1}{n} \sum_{i=1}^n \mathbb{D}_\alpha^K[\mathbb{P}_i, \cdot]$ . This is inspired by the work of [12]. Here, an image is considered as an empirical measure over a grid representing the intensity at each pixel in the image. We use a Gaussian kernel, and compute  $\mathbf{K}\mathbb{P}_i$  by convolving the image  $\mathbb{P}_i$  with an adequate filter, as proposed by [28]. The computation of the barycenter for each class requires less than 5 seconds on a single CPU, as compared to 90 seconds for the method proposed by [12, 13] implemented using a convolutional kernel [28]. Experimental details and comparison to [12, 13] can be found in Appendix D.

Finally, one can approximate a measure when the locations of the atoms are fixed. As an example, we take an article from the News Commentary Parallel Corpus [29], using as a measure  $\mathbf{p}$  the normalized TF-IDF weights of each non-stopword in the article. Here,  $\mathbf{K}$  is given by the normalized cosine similarity calculated over the 300-dimensional GLoVe [30] embeddings of each word. We optimize  $\mathbf{q}$  with gradient-based methods, applying a penalty to encourage sparsity. We show the result of this summarization in word-cloud format in Fig. 7. Experimental details are presented in Appendix D.3.



Figure 7: **Left:** The original word cloud. Word size is proportional to TF-IDF. **Center:** Our sparse approximation places mass only on 31 words. **Right:** Top 31 TF-IDF words in the original measure.

## 4.2 Measuring diversity

The GEAR entropy was originally proposed to quantify diversity in ecosystems [1], and similarly can be utilized to measure diversity in other data. The exponential of the entropy  $\exp(\mathbb{H}_\alpha^K[p])$  measures the effective number of points in the metric space under similarity  $\kappa_\sigma$  [9]. We empirically observe that varying  $\sigma$  allows us to identify the number of modes in simple examples such as mixtures of  $C$  Gaussians, shown in Fig. 8 where we observe that the entropy has a marked plateau at  $\mathbb{H}_\alpha^K[\mathbb{P}] = \log C$ .

For comparison, we adapt the birthday paradox-based approach of [31]. Strictly speaking, the method proposed by [31] requires human evaluation of possible duplicates, and is thus not comparable to our approach. As such, we propose an automated version using the same assumptions. We define  $\mathbf{x}$  and  $\mathbf{y}$  as colliding when  $d(\mathbf{x}, \mathbf{y}) < \epsilon$ , and note that the expected number of collisions for a distribution with support  $n$  in a sample of size  $m$  is  $c = \frac{m(m-1)}{n}$ . We can thus estimate  $\hat{n} = \frac{m(m-1)}{c}$ . When varying  $\epsilon$ , we observe behavior very similar to that of our entropy measure, with a plateau at  $\hat{n} = C$  in our example of a mixture of  $C$  Gaussians. The results of this comparison are presented in Fig. 8.

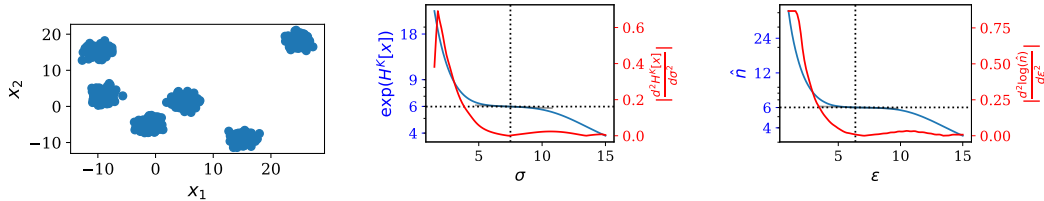


Figure 8: **Left:** 1000 sampled from a mixture of six Gaussians. **Center:** Modes detected by varying  $\sigma$  in our method. **Right:** The birthday paradox-based method. Note that the left axis is logarithmic.

To test this on a more challenging dataset, we use a 2-dimensional representation for MNIST [26] obtained using UMAP [32], shown in Fig. 9. Although our method no longer shows a clear plateau at  $\mathbb{H}_\alpha^K[\mathbb{P}] \approx \log 10 \approx 2.3$ , it does transition from exponential to linear decay at approximately this point, which coincides with the point of minimum curvature with respect to  $\sigma$ ,  $\mathbb{H}_\alpha^K[\mathbb{P}] \approx \log 10$ . Similar behavior is observed in the case with birthday-inspired estimate; here the point of minimum curvature has  $\hat{n} \approx 8$ . See further details in Appendix E.

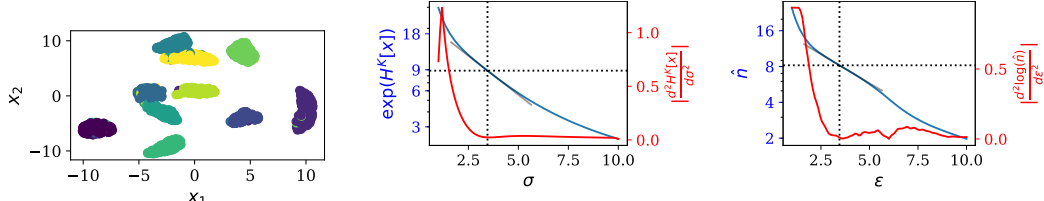


Figure 9: **Left:** A 2000-image subset of MNIST reduced to 2 dimensions by UMAP. **Center:** Our mode estimation. **Right:** The birthday paradox method estimate. Note that the left axis is logarithmic.

Finally, we also apply this method to evaluating the diversity of GAN samples. We train a simple WGAN [17] on MNIST, and find that the assessed entropy increases steadily as training progresses and the generator masters more modes (see Fig. 10). Note that the entropy estimate stabilizes once the generator begins to produce all 10 digits, but long before sample quality ceases improving.

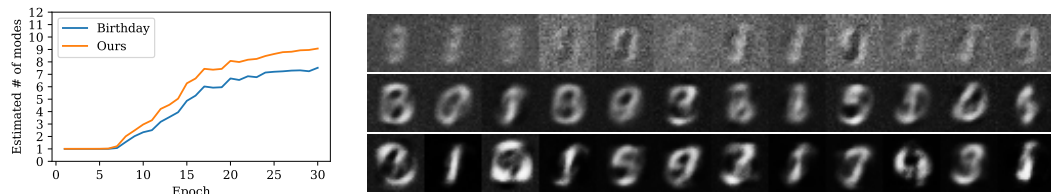


Figure 10: **Left:** The estimated numbers of modes in the output of a WGAN trained on MNIST. **Right:** Samples from the same WGAN after 5, 15 and 25 epochs.

### 4.3 Generative models

Generative models are trained to minimize a measure of disagreement between a distribution parameterized by the model and a target distribution [33, 16, 17]. In this section, we use  $\mathbb{D}_\alpha^K$  as an objective to train generative models on a toy Swiss roll data problem, as well as on the MNIST dataset. Fig. 11 (left, center) illustrate samples from the trained generative models. In particular, the learned manifold for MNIST digits exhibits a quality comparable to that reported in [33, Figure 4].

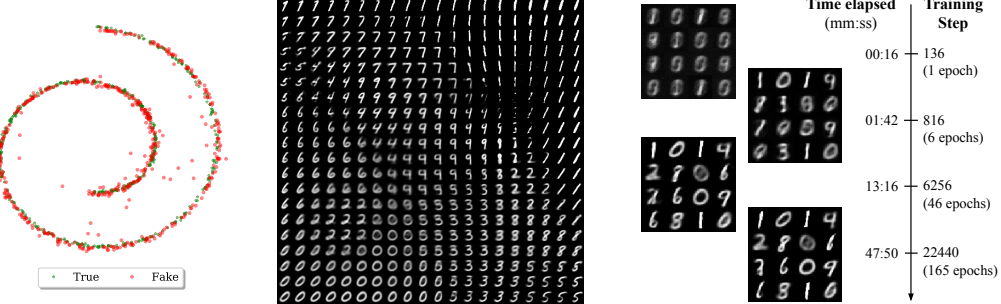


Figure 11: **Left:** Generated Swiss roll data. **Center:** Generated MNIST samples. **Right:** Intermediate MNIST samples during the generative model’s training.

Fig. 11 (right) shows samples generated during training of the model, along with time elapsed when the model is trained on a Nvidia TITAN Xp GPU with a batch size of 512. We observe that our model can generate reasonable and diverse images very early in training, within only a few hundred steps. This observation suggests that our objective provides a useful learning signal for the generator from the very beginning of optimization, which can be explained by the fact that we have a fixed kernel (without an adversarial component) and our loss is computed in closed form (without Sinkhorn iterations as in [18, 19]).

Historically, GANs have suffered from mode collapse, and a number of approaches have been proposed to counteract this behavior [34, 17]. Other generative models such as variational autoencoders [33] instead tend to have a mode covering behavior leading to blurry samples. Empirically, we observe that the hyperparameter  $\alpha$  in  $\mathbb{D}_\alpha^K$  allows us to control the trade-off between these behaviors. For small  $\alpha$ , our models tend to collapse to modes of the real distribution, whereas higher  $\alpha$  tend to produce higher diversity and more blurry images. We provide samples demonstrating this effect on the Swiss roll data in Appendix F.

## 5 Conclusions

We introduced the geometry-aware entropy originally proposed by [1] to the machine learning community and proposed the GEAR discrepancy: a similarity-sensitive loss inspired by this entropy. The GEAR discrepancy between two distributions can be computed efficiently in closed form, and generalizes the symmetric Rényi divergence. We performed a broad range of experiments with this loss, demonstrating its versatility.

The empirical results presented in this paper motivate further study of this new perspective on information theory. For instance, more exploration of the theoretical properties satisfied by the GEAR discrepancy is necessary, including investigating whether it is a divergence and what type of convergence of distributions it induces. Additionally, analysis of its sample complexity and bias for minibatch estimation would be desirable.

Finally, we note that the GEAR entropy is a non-increasing function of the similarities between the elements of the space, decreasing from the Rényi entropy when the kernel is identity to zero when the kernel is a matrix of ones. However, there might be multiple definitions of similarity-sensitive entropies satisfying the same conditions. Further study of an axiomatic characterization of this type of entropy could provide valuable insights into the theory of information on similarity spaces.

## Acknowledgments

This research was partially supported by the Canada CIFAR AI Chair Program and by a Google Focused Research award. We thank Pablo Piantanida for the great tutorial on information theory which inspired this work.

## References

- [1] T. Leinster and C. A. Cobbold, “Measuring diversity: The importance of species similarity,” *Ecology*, vol. 93, pp. 477–489, 3 2012.
- [2] A. Rényi, “On measures of entropy and information,” in *Proceedings of the Fourth Berkeley Symposium on Mathematical Statistics and Probability, Volume 1: Contributions to the Theory of Statistics*, The Regents of the University of California, 1961.
- [3] C. Shannon, “A mathematical theory of communication,” *The Bell System Technical Journal*, vol. 27, no. 3, pp. 379–423, 1948.
- [4] C. Villani, *Optimal Transport: Old and New*. Springer, 2008.
- [5] M. Cuturi, “Sinkhorn Distances: Lightspeed Computation of Optimal Transport,” in *Advances in Neural Information Processing Systems 26* (C. J. C. Burges, L. Bottou, M. Welling, Z. Ghahramani, and K. Q. Weinberger, eds.), pp. 2292–2300, Curran Associates, Inc., 2013.
- [6] N. Tishby and N. Zaslavsky, “Deep learning and the information bottleneck principle,” in *2015 IEEE Information Theory Workshop (ITW)*, pp. 1–5, IEEE, 4 2015.
- [7] R. Fox, A. Pakman, and N. Tishby, “Taming the Noise in Reinforcement Learning via Soft Updates,” in *Conference on Uncertainty in Artificial Intelligence*, 2016.
- [8] R. Reams, “Hadamard inverses, square roots and products of almost semidefinite matrices,” *Linear Algebra and its Applications*, vol. 288, pp. 35–43, 2 1999.
- [9] T. Leinster, “The magnitude of metric spaces,” *Documenta Mathematica*, 2013.
- [10] T. Leinster and M. W. Meckes, “Maximizing diversity in biology and beyond,” *Entropy*, vol. 18, p. 88, 3 2016.
- [11] I. Csiszár and P. C. Shields, “Information Theory and Statistics: A Tutorial,” *Foundations and Trends™ in Communications and Information Theory*, 2004.
- [12] M. Cuturi and A. Doucet, “Fast Computation of Wasserstein Barycenters,” in *International Conference on Machine Learning*, 2014.
- [13] J.-D. Benamou, G. Carlier, M. Cuturi, L. Nenna, and G. Peyré, “Iterative Bregman Projections for Regularized Transportation Problems,” *SIAM Journal on Scientific Computing*, vol. 37, no. 2, p. A1111–A1138, 2014.
- [14] S. Ben-David and S. Shalev-Shwartz, *Understanding Machine Learning: From Theory to Algorithms*. Cambridge University Press, 2014.
- [15] A. A. Alemi, B. Poole, I. Fischer, J. V. Dillon, R. A. Saurous, and K. Murphy, “Fixing a Broken ELBO,” in *International Conference on Machine Learning*, 2018.
- [16] I. J. Goodfellow, J. Pouget-Abadie, M. Mirza, B. Xu, D. Warde-Farley, S. Ozair, A. Courville, and Y. Bengio, “Generative Adversarial Nets,” in *Advances in Neural Information Processing Systems 27*, 2014.
- [17] M. Arjovsky, S. Chintala, and L. Bottou, “Wasserstein GAN,” tech. rep., 2017.
- [18] T. Salimans, H. Zhang, A. Radford OpenAI, and D. Metaxas, “Improving GANs Using Optimal Transport,” in *International Conference on Learning Representations*, 2018.
- [19] A. Genevay, G. Peyré, and M. Cuturi, “Learning Generative Models with Sinkhorn Divergences,” in *International Conference on Artificial Intelligence and Statistics*, vol. 84, 2018.

- [20] A. Smola, A. Gretton, L. Song, and B. Schölkopf, “A Hilbert Space Embedding for Distributions,” (Berlin, Heidelberg), pp. 13–31, Springer Berlin Heidelberg, 2007.
- [21] A. Gretton, K. M. Borgwardt, M. J. Rasch, A. Smola, B. Schölkopf, and A. Smola GRETTON, “A Kernel Two-Sample Test Bernhard Schölkopf,” *Journal of Machine Learning Research*, vol. 13, pp. 723–773, 2012.
- [22] A. Charpentier, “French dataset: population and GPS coordinates,” 2012.
- [23] F. Pedregosa, G. Varoquaux, A. Gramfort, V. Michel, B. Thirion, O. Grisel, M. Blondel, P. Prettenhofer, R. Weiss, V. Dubourg, J. Vanderplas, A. Passos, D. Cournapeau, M. Brucher, M. Perrot, and E. Duchesnay, “Scikit-learn: Machine Learning in Python,” *Journal of Machine Learning Research*, vol. 12, pp. 2825–2830, 2011.
- [24] Y. Chen, M. Welling, and A. Smola, “Super-samples from Kernel Herding,” in *Proceedings of the Twenty-Sixth Conference on Uncertainty in Artificial Intelligence*, UAI’10, (Arlington, Virginia, United States), pp. 109–116, AUAI Press, 2010.
- [25] S. Claici, E. Chien, and J. Solomon, “Stochastic Wasserstein Barycenters,” in *Proceedings of the 35th International Conference on Machine Learning* (J. Dy and A. Krause, eds.), vol. 80 of *Proceedings of Machine Learning Research*, (Stockholmsmässan, Stockholm Sweden), pp. 999–1008, PMLR, 2018.
- [26] Y. LeCun, L. Bottou, Y. Bengio, and P. Haffner, “Gradient-based learning applied to document recognition,” *Proceedings of the IEEE*, 1998.
- [27] H. Xiao, K. Rasul, and R. Vollgraf, “Fashion-MNIST: a Novel Image Dataset for Benchmarking Machine Learning Algorithms,” tech. rep., 2017.
- [28] J. Solomon, F. D. Goes, G. Peyré, M. Cuturi, A. Nguyen, T. Du, L. Guibas, J. Solomon, F. D. Goes, G. Peyré, M. Cuturi, A. Butscher, J. Solomon, and A. Butscher, “Convolutional Wasserstein Distances: Efficient Optimal Transportation on Geometric Domains,” *ACM Transactions on Graphics, Association for Computing Machinery*, 2015.
- [29] J. Tiedemann, “Parallel Data, Tools and Interfaces in OPUS,” in *LREC*, pp. 2214–2218, 2012.
- [30] J. Pennington, R. Socher, and C. Manning, “Glove: Global Vectors for Word Representation,” in *Conference on Empirical Methods in Natural Language Processing*, pp. 1532–1543, 2014.
- [31] S. Arora, A. Risteski, and Y. Zhang, “Do GANs Learn the Distribution? Some Theory and Empirics,” in *International Conference on Learning Representations*, pp. 1–16, 2018.
- [32] L. McInnes, J. Healy, and J. Melville, “UMAP: Uniform Manifold Approximation and Projection for Dimension Reduction,” tech. rep., 2018.
- [33] D. P. Kingma and M. Welling, “Auto-Encoding Variational Bayes,” in *International Conference on Learning Representations*, 2014.
- [34] T. Salimans, I. Goodfellow, W. Zaremba, V. Cheung, A. Radford, and X. Chen, “Improved techniques for training gans,” in *Advances in Neural Information Processing Systems*, pp. 2234–2242, 2016.
- [35] D. P. Kingma and J. Ba, “Adam: A Method for Stochastic Optimization,” in *International Conference on Learning Representations*, pp. 1–15, 2014.
- [36] A. Paszke, S. Gross, S. Chintala, G. Chanan, E. Yang, Z. DeVito, Z. Lin, A. Desmaison, L. Antiga, and A. Lerer, “Automatic differentiation in Pytorch,” in *Conference on Neural Information Processing Systems Autodiff Workshop*, vol. 22, pp. 2–8, 2017.
- [37] E. Loper and S. Bird, “NLTK: The Natural Language Toolkit,” in *Workshop on Effective tools and methodologies for teaching natural language processing and computational linguistics*, pp. 63–70, 2002.
- [38] M. J. E. Savitzky, Abraham; Golay, “Smoothing and Differentiation of Data by Simplified Least Squares Procedures,” *Analytical Chemistry*, vol. 36, no. 8, pp. 1627–1639, 1964.

- [39] I. Gulrajani, F. Ahmed, M. Arjovsky, V. Dumoulin, and A. C. Courville, “Improved Training of Wasserstein GANs,” in *Advances in Neural Information Processing Systems 30* (I. Guyon, U. V. Luxburg, S. Bengio, H. Wallach, R. Fergus, S. Vishwanathan, and R. Garnett, eds.), pp. 5767–5777, Curran Associates, Inc., 2017.
- [40] S. Ioffe and C. Szegedy, “Batch Normalization: Accelerating Deep Network Training by Reducing Internal Covariate Shift,” in *Proceedings of the 32nd International Conference on Machine Learning - Volume 37*, ICML’15, pp. 448–456, JMLR.org, 2015.

## A Revisiting parallel lines

Let  $Z \sim \mathcal{U}([0, 1])$ ,  $\phi \in \mathbb{R}$ , and let  $\mathbb{P}_\phi$  be the distribution of  $(\phi, Z) \in \mathbb{R}^2$ , i.e., a (degenerate) uniform distribution on the segment  $\{\phi\} \times [0, 1] \subset \mathbb{R}^2$ , illustrated in Fig. 12.

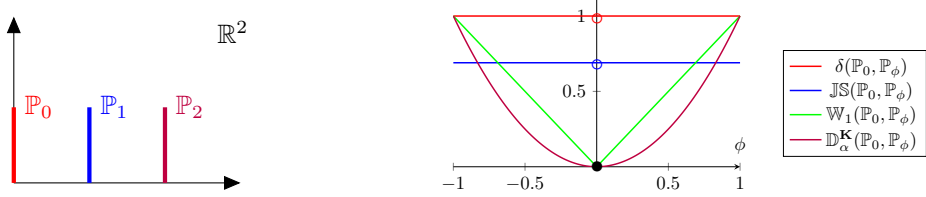


Figure 12: Degenerate distribution  $\mathbb{P}_\phi$  over the segment  $\{\phi\} \times [0, 1]$  for different values of  $\phi$ .

Figure 13: Values of the divergences as functions of  $\phi$ . KL divergence values are  $\infty$  except at  $\phi = 0$ .

Our goal is to find the *right* value of  $\phi$  for a model distribution  $\mathbb{P}_\phi$  using the dissimilarity with respect to a target distribution  $\mathbb{P}_0$  as a learning signal. The behavior of common divergences on this type of problem was presented by [17] as a motivating example for the introduction of OT distances in the context of GANs.

$$\begin{aligned} \delta(\mathbb{P}_0, \mathbb{P}_\phi) &= \begin{cases} 0 & \text{if } \phi = 0 \\ 1 & \text{else} \end{cases} & \text{KL}(\mathbb{P}_0, \mathbb{P}_\phi) &= \text{KL}(\mathbb{P}_\phi, \mathbb{P}_0) = \begin{cases} 0 & \text{if } \phi = 0 \\ \infty & \text{else} \end{cases} \\ \mathbb{W}_1(\mathbb{P}_0, \mathbb{P}_\phi) &= |\phi| & \text{JS}(\mathbb{P}_0, \mathbb{P}_\phi) &= \log(2) \delta(\mathbb{P}_0, \mathbb{P}_\phi) \end{aligned} \quad (4)$$

Note that among all these divergences, only the Wasserstein distance provides a continuous (even a.e. differentiable) objective on  $\phi$ . See Fig. 13.

Study the behavior of our loss:

$$\mathbb{D}_\alpha^{\mathbf{K}}(\mathbb{P}_0, \mathbb{P}_\phi) = \frac{1}{2} \frac{1}{\alpha-1} \left[ \log \left( \mathbb{E}_{(x,y) \sim \mathbb{P}_0} \left[ \frac{\mathbf{K}\mathbb{P}_0(x,y)}{\mathbf{K}\mathbb{P}_\phi(x,y)} \right]^{\alpha-1} \right) + \log \left( \mathbb{E}_{(x,y) \sim \mathbb{P}_\phi} \left[ \frac{\mathbf{K}\mathbb{P}_\phi(x,y)}{\mathbf{K}\mathbb{P}_0(x,y)} \right]^{\alpha-1} \right) \right]$$

Recall that the action of the kernel on a given probability measure corresponds to the mean map  $\mathbf{K}\mu : \mathcal{X} \rightarrow \mathbb{R}$ , defined by  $\mathbf{K}\mu(x) \triangleq \mathbb{E}_{x' \sim \mu} [\kappa(x, x')] = \int \kappa(x, x') d\mu(x')$ . In particular, for  $\mathbb{P}_\phi$ :

$$\mathbf{K}\mathbb{P}_\phi(x, y) = \int_{\mathbb{R}^2} \kappa((x, y), (x', y')) d\mathbb{P}_\phi(x', y') = \int_0^1 \kappa((x, y), (\phi, y')) dy'.$$

Let us endow  $\mathbb{R}^2$  with the Euclidean norm  $\|\cdot\|$ , and define the kernel  $\kappa((x, y), (x', y')) \triangleq \exp(-\|(x, y) - (x', y')\|^2)$ . For this choice of kernel, the mean map reduces to:

$$\mathbf{K}\mathbb{P}_\phi(x, y) = \int_0^1 \exp[-((x - \phi)^2 + (y - y')^2)] dy' = \exp[-(x - \phi)^2] \underbrace{\int_0^1 \exp[-(y - y')^2] dy'}_{\triangleq I_y, \text{ independent of } \phi}.$$

Thus, we obtain the following expression for the expectations in the definition of the loss:

$$\mathbb{E}_{(x,y) \sim \mathbb{P}_\eta} \left[ \frac{\mathbf{K}\mathbb{P}_\eta(x,y)}{\mathbf{K}\mathbb{P}_\theta(x,y)} \right]^{\alpha-1} = \mathbb{E}_{(x,y) \sim \mathbb{P}_\eta} \left[ \frac{\exp[-(x - \eta)^2]}{\exp[-(x - \theta)^2]} \mathbb{I}_\mathcal{X} \right]^{\alpha-1} = \exp[(\alpha - 1)(\eta - \theta)^2].$$

Putting all the pieces together:

$$\begin{aligned} \mathbb{D}_\alpha^{\mathbf{K}}(\mathbb{P}_0, \mathbb{P}_\phi) &= \frac{1}{2} \frac{1}{\alpha-1} \left[ \log \left( \mathbb{E}_{(x,y) \sim \mathbb{P}_0} \left[ \frac{\mathbf{K}\mathbb{P}_0(x,y)}{\mathbf{K}\mathbb{P}_\phi(x,y)} \right]^{\alpha-1} \right) + \log \left( \mathbb{E}_{(x,y) \sim \mathbb{P}_\phi} \left[ \frac{\mathbf{K}\mathbb{P}_\phi(x,y)}{\mathbf{K}\mathbb{P}_0(x,y)} \right]^{\alpha-1} \right) \right] \\ &= \frac{1}{2} \frac{1}{\alpha-1} [(\alpha-1)(0 - \phi)^2 + (\alpha-1)(\phi - 0)^2] \\ &= \phi^2. \end{aligned}$$

Remarkably, this result is independent of  $\alpha$  and is a smooth function of the parameter  $\phi$ .

## B Finding maximum entropy distributions with gradient descent

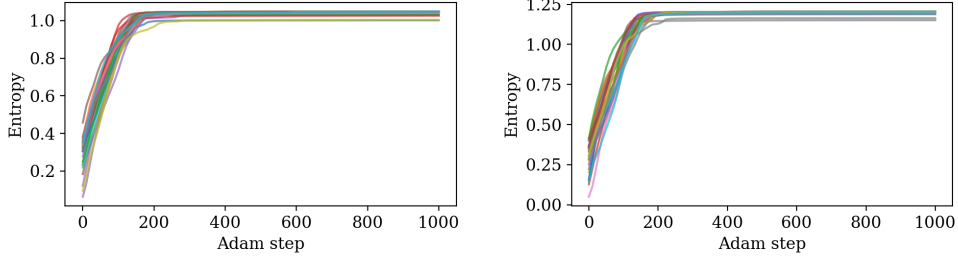


Figure 14: Optimization curves for measures with support 1000 in dimension 5 (left) and 100 (right).

In this section, we test our ability to find maximum GEAR entropy distributions via gradient descent. We sample 1000 points in dimensions 5 and 10, and construct a similarity space using a RBF kernel with  $\sigma = 1$ . We perform 100 trials by setting the logits of the initialization using a Gaussian with variance 10 for each of the 1000 weights that describe our distribution. In every trial we sample a new  $\alpha$  uniformly between 0 and 5, to confirm that the value of the maximum entropy is independent of  $\alpha$ . We use Adam [35] with learning rate 0.05. The optimization results are shown in Fig. 14. We observe that initializing the distributions close to uniform (smaller variance for sampling the initial logits) yields even smaller variance in the optimization across trials.

## C Non-negativity of GEAR discrepancy

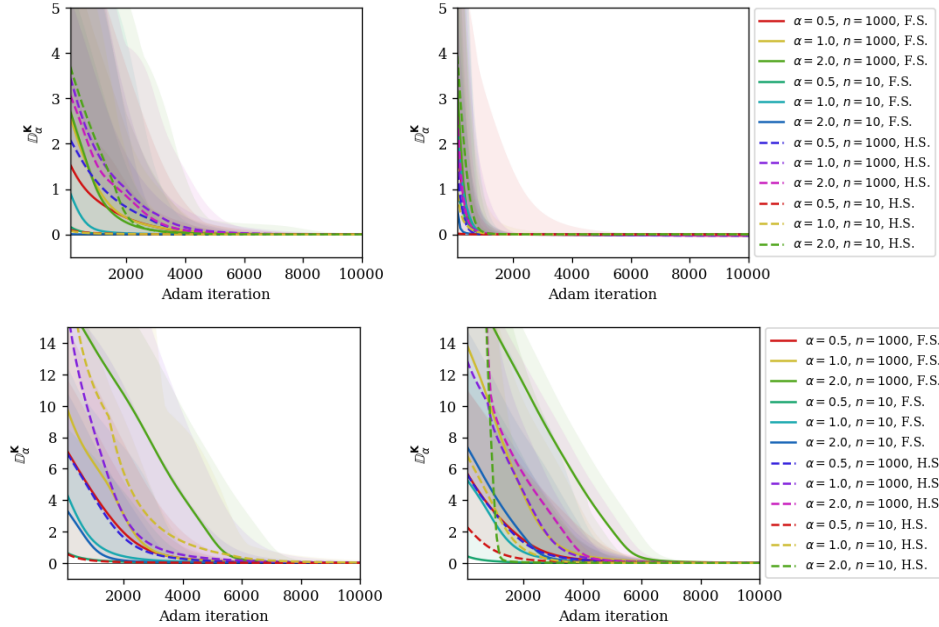


Figure 15: Optimization curves for the standard RBF kernel. **Top row:** Locations in  $\mathbb{R}^5$ . **Bottom row:** Locations in  $\mathbb{R}^{100}$ . **Left column:** Optimization with  $\mathbf{p}$  fixed. **Right column:** Joint optimization over  $\mathbf{p}$  and  $\mathbf{q}$ .

We hypothesize that  $\mathbb{D}_\alpha^K(\mathbf{p}, \mathbf{q})$  is a non-negative discrepancy between distributions. To investigate this empirically, we consider two empirical distributions  $\mathbf{p}$  and  $\mathbf{q}$  over points in both  $\mathbb{R}^5$  and  $\mathbb{R}^{100}$ . We also consider two kernels defining the geometry of the space: a RBF kernel and a polynomial kernel  $\kappa(\mathbf{x}, \mathbf{y}) \triangleq \frac{1}{1 + \|\mathbf{x} - \mathbf{y}\|^2}$ . We minimize the discrepancy by changing the locations of the atoms

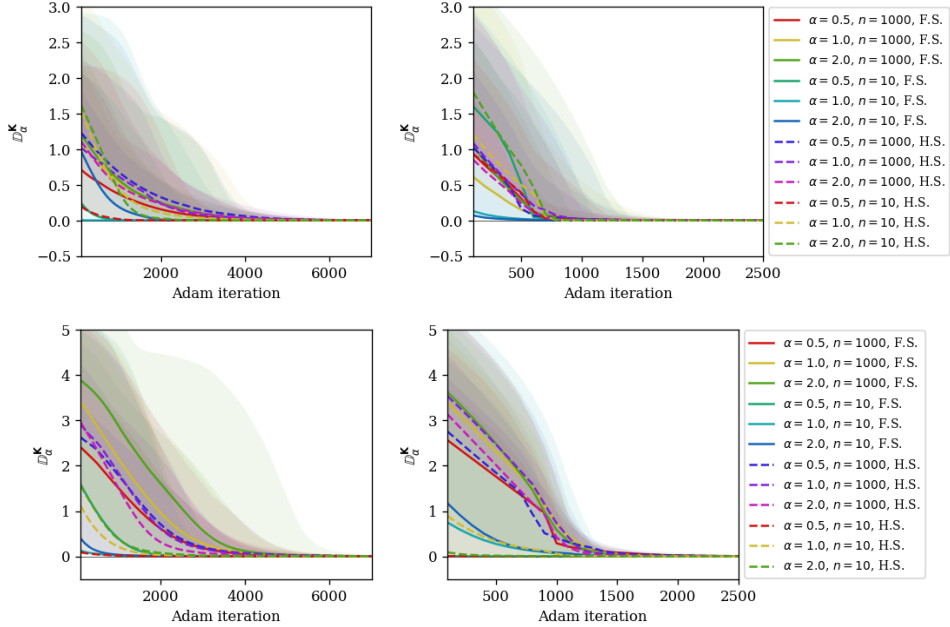


Figure 16: Optimization curves for the polynomial kernel. **Top row:** Locations in  $\mathbb{R}^5$ . **Bottom row:** Locations in  $\mathbb{R}^{100}$ . **Left column:** Optimization with  $\mathbf{p}$  fixed. **Right column:** Joint optimization over  $\mathbf{p}$  and  $\mathbf{q}$ .

of each measure as well as their weights (both jointly over  $\mathbf{p}$  and  $\mathbf{q}$  and fixing the weights of  $\mathbf{p}$  and modifying only those of  $\mathbf{q}$ ). The weights of  $\mathbf{p}$  and  $\mathbf{q}$  are parametrized with a softmax function applied to vectors of logits. Since this parametrization induces full support in the distributions we additionally designed experiments in which  $\mathbf{p}$  is restricted to have support over only  $n/2$  elements, denoted as H.S. in Fig. 15 and 16. This allows us to consider distributions on the boundary of the simplex in our search.

We vary values of  $\alpha$  in  $\{0.5, 1, 2\}$  and  $n$  in  $\{10, 1000\}$  and perform this optimization using the Adam optimizer [35]. Each setting is run 10 times, and we report the minimum (solid lines) and maximum values (shaded regions indicate the range) at every step of optimization across runs in Fig. 15 for the RBF kernel and in Fig. 16 for the polynomial kernel. H.S. and F.S. indicate experiments with half support and full support for  $\mathbf{p}$ , respectively. We see that all experiments converge around zero.

## D Interpolation and Approximation

In all experiments for Figs. 4-6, we minimize the GEAR discrepancy using the Adam optimizer [35] in PyTorch [36]. We parameterize the weights of empirical distributions using a softmax function on a vector of temperature-scaled logits. All experiments in the section are run on a single CPU.

### D.1 Approximating measures with finite samples

In Fig. 4, we approximate a discrete measure using a finite number of samples using a discrepancy of order  $\alpha = 0.5$ . We train using Adam for 3000 steps with a learning rate of  $10^{-3}$  and minibatches constructed by sampling 50 examples at each step. We use a Gaussian kernel with  $\sigma = 0.02$ .

In Fig. 5, we approximate a continuous measure with a finite number of atoms. We set  $\alpha = 0.5$  and execute Adam for 500 steps using a learning rate of 0.05 and minibatches of 100 samples from the continuous measure to estimate the discrepancy. The similarity function is given by a polynomial kernel with exponent 1.5:  $\kappa(\mathbf{x}, \mathbf{y}) \triangleq \frac{1}{1 + \|\mathbf{x} - \mathbf{y}\|^{1.5}}$ .

## D.2 Image barycenters

We compute barycenters for each class of MNIST and Fashion-MNIST. We perform gradient descent with Adam using a learning rate of 0.01 with minibatches of size 32 for 500 optimization steps. The order of the discrepancy is  $\alpha = 1.5$ . We use a Gaussian kernel with  $\sigma = 0.04$ . The geometry of the grid on which images are defined is given by the Euclidean distance between the coordinates of the pixels. In Fig. 17, we provide barycenters for the classes of MNIST computed via a combination of the methods of [13] and [12]. We note that the quality of these barycenters is comparable to ours, although ours are slightly sharper.



Figure 17: Barycenters for MNIST computed using the method of [12].

## D.3 Text summarization

For our text example, we use the article from the STAT-MT parallel news corpus titled “Why Wait for the Euro?”, by Leszek Balcerowicz. The full text of the article can be found at <https://pastebin.com/CnBgbpsJ>. We use the 300-dimensional GLoVe vectors found at <http://nlp.stanford.edu/data/glove.6B.zip> as word embeddings. TF-IDF is calculated over the entire English portion of the parallel news corpus using the implementation in Scikit-Learn [23]. We filter stopwords based on the list provided by the Natural Language Toolkit [37]. To encourage sparsity in the approximating measure  $\mathbf{q}$ , we add the 0.75-norm of  $\mathbf{q}$  to the divergence loss, weighted by a factor of 0.01. We optimize the loss with gradient descent using the Adam optimizer [35] in PyTorch [36], with hyperparameters  $\beta_1 = 0$ ,  $\beta_2 = 0.9$ ,  $\alpha = 0.001$ , for 25,000 iterations. Since a truly sparse  $\mathbf{q}$  is not reachable using the softmax function and gradient descent, we set all entries  $q_i < 0.01$  to be 0 and renormalize after training completes.  $\mathbf{q}$  is represented by the softmax function, and is initialized to match  $\mathbf{p}$ . We use a value of  $\alpha = 1$  in  $\mathbb{D}_\alpha^K$ .

## E GAN evaluation and mode counting

In all of the experiments corresponding to mode counting, we use  $\alpha = 1$  and the standard RBF kernel  $\kappa_\sigma(\mathbf{x}, \mathbf{y}) = \exp\left(\frac{-\|\mathbf{x}-\mathbf{y}\|^2}{2\sigma^2}\right)$ . Note that this differs from the kernel given in Section 2 by using squared Euclidean distance rather than Euclidean distance. To estimate the point with minimum curvature, we find the value of  $\log \hat{n}$  or  $\mathbb{H}_\alpha^K \mathbf{p}$  at 100 values of  $\sigma$  or  $\epsilon$  evenly spaced between 0.1 and 25, and empirically estimate the second derivative with respect to  $\sigma$  or  $\epsilon$ . In the case of the birthday estimate, which is not continuous on finite sample sizes, we use a Savitzky-Golay filter [38] of degree 3 and window size 11 to smooth the derivatives. We estimate the point of minimum curvature to be the first point when the absolute value of the second derivative passes below 0.01.

To evaluate GANs, we train a simple WGAN-GP [39] with a 3-hidden-layer fully-connected generator, using the ReLU nonlinearity and 256 units in each hidden layer, on a TITAN Xp GPU. Our latent space has 32 dimensions sampled i.i.d. from  $\mathcal{N}(0, 1)$  and the discriminator is trained for four iterations for each generator update. We use the Adam optimizer [35] with learning rate  $10^{-4}$  and  $\beta_1 = 0$ ,  $\beta_2 = 0.9$ . The weight of the gradient penalty in the WGAN-GP objective is set to  $\lambda = 10$ .

To count the number of modes in the output of the generator, we use an instance of UMAP fitted to the entire training set of MNIST to embed all input in  $\mathbb{R}^2$ . We use 1,000 samples of true MNIST data to estimate values of  $\sigma$  (for our entropy method) and  $\epsilon$  for the birthday paradox-based method that minimize curvature and yield estimates of  $\exp \mathbb{H}_\alpha^K \mathbf{p} \approx 10$  and  $\hat{n} \approx 10$ . We then apply these methods to the output of the generator after each of the first 30 epochs, and report the resulting  $\hat{n}$  or  $\exp \mathbb{H}_\alpha^K \mathbf{p}$ .

## F Generative models

We employ a multilayer perceptron with two hidden layers with 256 dimensions as the pushforward on  $\mathcal{N}(0, \mathbf{I})$  in  $\mathbb{R}^{16}$  to  $\mathbb{R}^2$  to match the Swiss roll data by minimizing  $\mathbb{D}_1^K$  using a RBF kernel with  $\sigma = 0.2$ . For MNIST, we use a multilayer perceptron with two hidden layers with 384 dimensions each as the pushforward on  $[0, 1]^2$  to the MNIST image space  $[0, 1]^{28 \times 28}$ , minimizing  $\mathbb{D}_2^K$  using a RBF kernel with  $\sigma = 4.6$ . Both models are trained using the Adam optimizer and use batch normalization [40]. Furthermore, for the MNIST experiment, we take gradients with respect to  $2\mathbb{D}_\alpha^K(\hat{\mathbb{P}}, \hat{\mathbb{Q}}) - \mathbb{D}_\alpha^K(\hat{\mathbb{P}}, \hat{\mathbb{P}}') - \mathbb{D}_\alpha^K(\hat{\mathbb{Q}}, \hat{\mathbb{Q}}')$ , where  $\hat{\mathbb{P}}, \hat{\mathbb{P}}'$  are two i.i.d. samples from the data distribution, and  $\hat{\mathbb{Q}}, \hat{\mathbb{Q}}'$  are i.i.d. samples from the pushforward on the latent code distribution, in the spirit of a generalized energy distance as proposed in [18, 19], accounting for biased gradients due to taking the logarithm of an expectation over minibatches in Equation 2. Note that although we report results using a fixed RBF kernel, our generative models can also be trained along with learned kernels by using an adversarial setup similar to [18].

**Controlling mode collapse.** We observe that changing values of  $\alpha$  in  $\mathbb{D}_\alpha^K$  lets us control the trade-off between mass covering and mode collapsing behavior of our generators. To illustrate this effect, we train generative models by minimizing  $\mathbb{D}_\alpha^K$  with  $\alpha \in \{10^{-4}, 1, 5\}$  between the Swiss roll data and a generator distribution, and report the results in Fig. 18. The configuration of the generator network and the optimization hyperparameters are identical to those above. These results suggest that setting schedules on  $\alpha$  (potentially a damped oscillatory behavior alternating between larger and smaller values) can help improve the mode covering behavior of generative models.

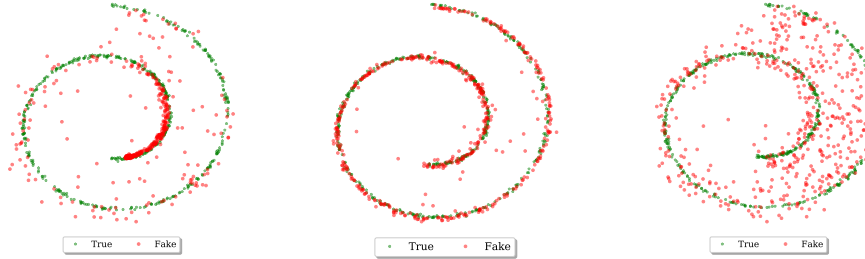


Figure 18: Samples from generative models trained on Swiss roll data with different values of  $\alpha$ . **Left:**  $\alpha = 10^{-4}$ . **Center:**  $\alpha = 1$ . **Right:**  $\alpha = 5$ .